Bead-Pull Measurements of the Main Deflecting Mode of the Double-Quarter-Wave Cavity for the HL-LHC

M. Navarro-Tapia, R. Calaga, CERN, Geneva, Switzerland

Introduction

The novel machine configuration of the LHC, called High-Luminosity LHC (HL-LHC) [1], will rely on a number of innovative technologies, such as the use of superconducting deflecting cavities for beam rotation (crab cavities). These cavities are designed to deflect/crab the beam at 400 MHz [2], where the transverse kick results from the interaction of the particle with both the transverse electric and magnetic fields. The double-quarter-wave (DQW) cavity [3] is one of the candidates to be considered. the first RF tests that have been carried out on a full-scale aluminum prototype of the DQW cavity. The RF characterization of the fundamental deflecting mode, for both the transverse and longitudinal electromagnetic fields, has been done by means of bead-pull measurements.

Prototype description

The cavity geometry can be seen as a double $\lambda/4$ line with symmetric poles –also referred to as "domes"– to create a transverse electric field and cancel any longitudinal field. The deflection in this case is mainly due to the strong transverse electric field between these parallel domes. The aperture of the domes is equal to the diameter of the incoming and outgoing beam pipes (ID=42 mm).The first higher-order mode is resonating at $\sim$578 MHz, around 180 MHz apart from the fundamental mode. This mode only has a longitudinal component of the electric field on axis, which will be useful when calibrating the longitudinal form factor of any needle-like perturbing object.
A full-scale prototype of the DQW cavity –made out of aluminum– has been built at CERN to carry out the first RF measurements. Figure below shows a picture of the prototype, with the beam-pipe axis lying vertically. The drawings with the exact dimensions of this prototype can be found in [4].

Deflecting-Mode Field Distribution

Figure below shows both the on-axis and the off-axis field magnitude of the different components of the electric field, $|E_n|$, and the magnetic field, $|H_n|$, where n denotes the corresponding coordinate (x, y or z). The magnetic field is represented multiplied by the free-space impedance, $\eta_0 \approx 120\,\pi$, in order to establish a fair comparison of the respective contribution of the electric and magnetic fields to the transverse kick. Note that all the components are normalized to the square root of the stored energy, $\sqrt{U}$.

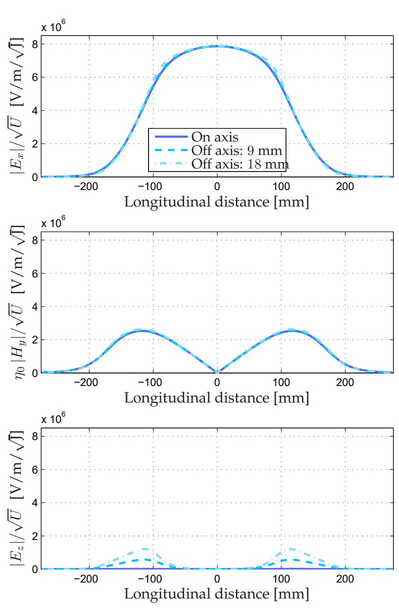

Small-Perturbation Theorem

Under this assumption of small perturbation, the frequency shift of the cavity resonance is given by [7, 8, 9]:

$$\frac{\Delta\omega}{\omega_0} = \alpha_{E_\perp}\varepsilon_0\frac{|E_\perp|^2}{U} + \alpha_{E_\parallel}\varepsilon_0\frac{|E_\parallel|^2}{U} + \alpha_{H_\perp}\mu_0\frac{|H_\perp|^2}{U} + \alpha_{H_\parallel}\varepsilon_0\frac{|H_\parallel|^2}{U}, \tag{1}$$

where ε_0 and μ_0 are the vacuum permittivity and permeability, respectively; and $E_\perp$, $E_\parallel$, $H_\perp$ and $H_\parallel$ are the electric and magnetic fields perpendicular and parallel to the perturbing object. The coefficients $\alpha_{E_\perp}$, $\alpha_{E_\parallel}$, $\alpha_{H_\perp}$ and $\alpha_{H_\parallel}$ are the form factors associated to the respective fields, and they are proportional to the electric and magnetic polarizability of the perturbing object.

Bead-Pull Measurements

A small bead is pulled along ab arbitrary path through the cavity while the resonance frequency is being monitored as a function of the position of the object. It is more accurate to measure the frequency shift by measuring the phase shift of a transmitted signal at the resonance frequency [10]. Because of the non-linearity of the tan function, $\Delta\phi$ should be kept small enough (in practice, $\Delta\phi \lesssim 25°$). Figure below shows the bead-pull measurement setup used. The software to run the bead-pull measurements is encoded in LabVIEW [11]. This nylon wire carrying the bead is arranged in a closed loop.

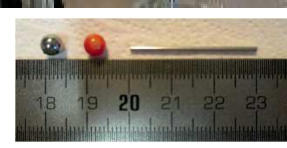

Two types of perturbing objects have been chosen (see sigure above. The sphere is chosen to measure the transverse components of the electromagnetic fields, both $E_\perp$ and $H_\perp$. A metallic and a dielectric (stone) spheres of diameter 5 mm have been used. Unlike the non-directional sphere, the elongated shape of needle makes it more coupled to the longitudinal electric fields than to the transverse ones. Therefore, the needle is chosen as a perturbing object to measure the longitudinal components of the electric field, E_z. A 30-mm long needle with cylindrical shape (diameter 1.2 mm) has been used.
Because of the non-directional geometry of the sphere, the perturbation effect becomes also non-directional as well, and the frequency shift becomes:

$$\frac{\Delta\omega}{\omega_0} = -\pi r^3\,\varepsilon_0\frac{|E_\perp|^2}{U} + \frac{1}{2}\pi r^3\,\mu_0\frac{|H_\perp|^2}{U}, \tag{2}$$

where r is the radius of the sphere. From In order to be able to separate both components, a dielectric (stone) sphere is used. It will only interact with the electric field in the following way:

$$\frac{\Delta\omega}{\omega_0} = -\pi r^3\frac{\varepsilon_r - 1}{\varepsilon_r + 2}\varepsilon_0\frac{|E_\perp|^2}{U}, \tag{3}$$

where ε_r is the relative permittivity of the material.

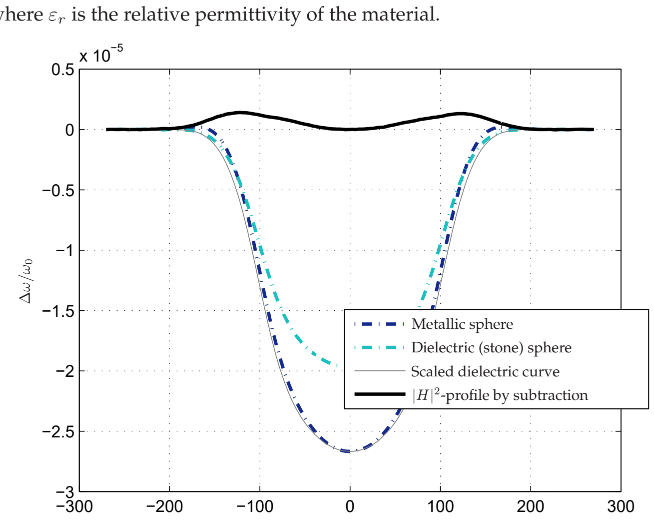

Figure above shows together the measurements coming from the metallic and the dielectric spheres, in the form of $\Delta\omega/\omega_0$ *versus* longitudinal distance. The averaged curves calculated over 30 measurements are shown. For the metallic sphere, $\Delta\omega/\omega_0 > 0$ at around $z = \pm 150$ mm, due to the contribution of H_y. The magnetic field contribution is can be found from the difference between the two measurements [12, 13].

Transverse Components

The squared magnetic-field profile is obtained by subtracting the scaled measurements of the dielectric sphere from the measurements of the metallic sphere. The subtracted trace is plotted as a black continuous line in the previous figure. The calibration of the form factors of the different spheres has been done by doing on-axis measurements of the fundamental mode of the DQW cavity. A comparison between the measured fields and the simulated ones is shown in Figures below A reasonably good matching between simulations and measurements can be observed, specially if considering that these values of the magnetic field are an order of magnitude below the electric field.

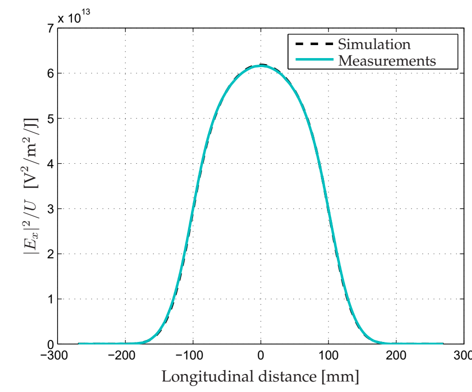

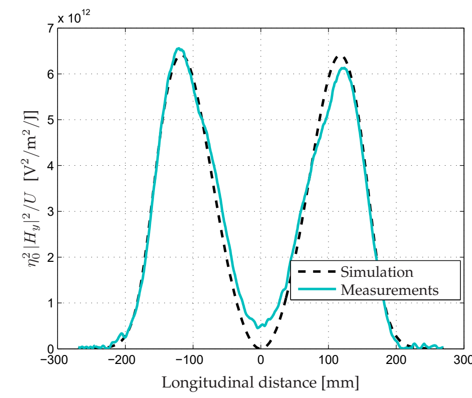

1 Longitudinal Components

Due to the finite cross section of the needle and the strong transverse fields compared to the longitudinal ones, the effect of the transverse fields are also picked up in the measurements using a needle. The frequency shift in this particular case of a needle off-axis in the DQW is given by:

$$\frac{\Delta\omega}{\omega_0} = \alpha_{E_{n\perp}}\varepsilon_0\frac{|E_\perp|^2}{U} + \alpha_{E_{n\parallel}}\varepsilon_0\frac{|E_\parallel|^2}{U} + \alpha_{H_{n\perp}}\mu_0\frac{|H_\perp|^2}{U}, \tag{4}$$

where the subscript n stands for "needle".

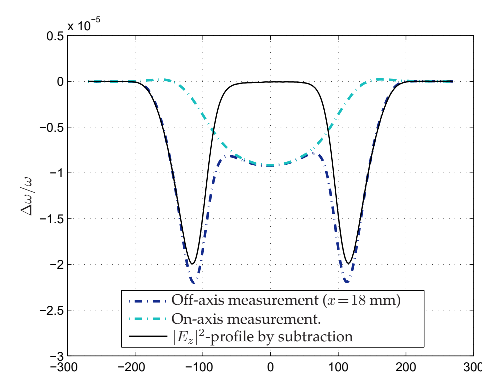

Figure above shows together the on-axis and off-axis (18 mm) measurements done with the needle, in the form of $\Delta\omega/\omega_0$ *versus* longitudinal distance averaged over 30 measurements. With the off-axis measurements, the contribution of the transverse E_x is measured. Assuming that the transverse fields on-axis have a negligible variation across the beam-pipe cross section, the off-axis measurements at the center of the cavity exactly overlap with the on-axis measurements. Therefore, the longitudinal electric field can be profiled just by subtracting the on-axis measurement from the off-axis one, as illustrated in Figure above. To calibrate the needle, bead-pull measurements with the first higher-order mode of the DQW cavity have been done. This is a longitudinal mode with a very convenient field distribution. Figure below shows a comparison between the measured fields and the simulated ones, where the squared values of the normalized fields are plotted. A good matching between simulation and measurements is found.

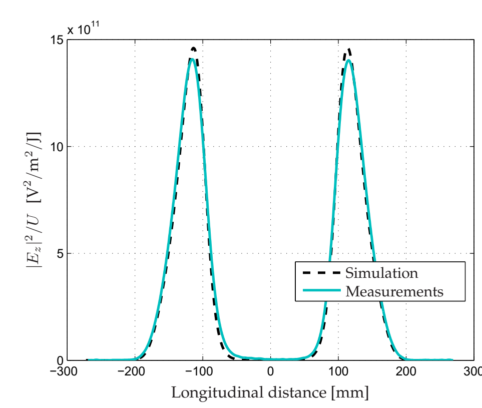

References

[1] High Luminosity LHC, `http://hilumilhc.web.cern.ch`
[2] P. Baudrenghien et al., CERN-ACC-NOTE-2013-003, February 2013.
[3] I. Ben-Zvi et al., presented at 5th LHC CC Workshop, Geneva, 2011.
[4] T. Renaglia, `https://edms.cern.ch/document/1245841/0`.
[5] HFSS, version 15.0, ANSYS Inc., Canonsburg, PA.
[6] W. K. H. Panofsky, and W. A. Wenzel, Rev. of Sci Inst., vol. 27, p. 967, 1956.
[7] L. C. Maier, and J. C. Slater, J. of Applied Physics, vol. 3, no. 1, Jan. 1952.
[8] Edward L. Ginzton, *Microwave Measurements*, New York: McGraw-Hill, 1957.
[9] J. C. Slater, *Microwave Electronics*, New York: D. Van Nostrand Company, Inc., 1950.
[10] F. Caspers and G. Dôme, in *Proc. of Conference on Precision Electromagnetic Measurements*, Delft, The Netherlands, 1984.
[11] LabVIEW, version 2013. National Instruments, Austin, USA. `http://www.ni.com/labview`.
[12] B. Hall, PhD dissertation, Sep. 2012.
[13] D. Alesini et al., NIMA, vol. 568, pp. 488-502, 2006.